PERGAMON

International Journal of Solids and Structures 39 (2002) 3387–3408

INTERNATIONAL JOURNAL OF SOLIDS and STRUCTURES

www.elsevier.com/locate/ijsolstr

Dynamics of non-isothermal martensitic phase transitions and hysteresis

Anna Vainchtein

Department of Mathematics, University of Pittsburgh, 301 Thackeray Hall, Pittsburgh, PA 15260, USA

Received 13 February 2002

Abstract

We consider a non-isothermal one-dimensional model of martensitic phase transitions that incorporates a finite bar with a non-monotone temperature-dependent stress–strain law and non-zero latent heat. Two dissipation mechanisms are considered: heat conduction and the internal viscous dissipation of kinetic origin. Time-dependent displacement and ambient temperature are prescribed at the ends of the bar. Numerical simulations of this model predict both rate-independent hysteresis, which persists at slow loading, and the rate-dependent portion due to thermal effects. The loops possess serrations caused by nucleation and annihilation events and the motion of interfaces. We observe that when heat conductivity is large, or the applied loading is sufficiently slow, the results are similar to those of Vainchtein and Rosakis [Journal of Nonlinear Science 9 (6) (1999) 697] for the isothermal case, with serrated loops accompanied by nucleations and stick–slip motion of phase boundaries. At faster loading and smaller heat conductivity (or larger latent heat), the stick–slip interface motion is partially replaced by irregular slow–fast interface motion and damped temporal oscillations in both released heat and end load. We show that at higher loading rates more interfaces are formed, and the phase transition causes self-heating of the bar, in qualitative agreement with experimental observations.

Keywords: Phase transitions; Pseudoelastic hysteresis; Latent heat; Heat conduction; Thermoviscoelasticity

1. Introduction

Shape memory alloys (for example, NiTi, CuAlNi) is a class of smart materials that has attracted a lot of attention during the last 20 years. One of the remarkable properties exhibited by these materials is called *pseudoelasticity* and refers to the ability of the material in a certain temperature regime to accommodate large deformations (up to 8% strain) during isothermal mechanical loading and then completely recover upon unloading. When subjected to a cycling loading, the material exhibits *hysteresis*, thus absorbing and releasing large amounts of energy. A possible practical application of this property is vibration damping where the shape memory materials have been shown to be much more effective than the conventional alloys used for this purpose (Li and Feng, 1997). Other applications include eyeglass frames, medical guide wires

E-mail address: annav@math.pitt.edu (A. Vainchtein).

0020-7683/02/$ - see front matter
PII: S0020-7683(02)00160-9

and arch wires for orthodontic correction. The underlying mechanism for pseudoelasticity is the transformation, induced by the loading, from austenite to martensite material phases, and the formation and motion of phase boundaries. Frequently, a finely layered microstructure containing alternating layers of both phases is formed in the process.

In his pioneering work, Ericksen (1975) has shown the fundamental importance of a non-convex elastic energy for the hysteretic behavior of crystalline solids. This approach was then further developed and led to the important contributions by a number of researchers (see James, 1992, for a review). In addition, many interesting experimental results were obtained (Chu, 1993; Leo et al., 1993; Shaw and Kyriakides, 1995; Shield, 1995). While a significant progress has been made, in particular, in understanding the basic features of microstructure, some phenomena are still not completely understood.

Some of the questions that remain to be fully addressed are the dynamics of phase boundaries, the origin of pseudoelastic hysteresis and the development of a relatively simple model capable of predicting the size and features of the experimentally observed hysteresis loops. Recent experiments (Leo et al., 1993; Shaw and Kyriakides) clearly indicate that such a model must necessarily account for the strong coupling between the deformation and thermal fields. While the experiments are conducted isothermally, *locally* the temperature experiences significant changes during both nucleation and phase boundary motion, due to the latent heat of the transformation. This leads to the phenomenon of *self-heating* (self-cooling) during loading (unloading). The observed hysteresis loops thus consist of two parts: the *isothermal* (or quasistatic) portion, which does not depend on the loading rate, and the *rate-dependent* portion which is due to the thermal effects. [1] Both experimental work and recent numerical simulations (Bubner, 1996; Shaw, 2000) point out the importance of *coupling* between the temperature and deformation as a key to a better understanding of hysteretic behavior in shape memory alloys subjected to cyclic loading.

Until recently, most work on the dynamics of phase transitions in a finite bar has concentrated on either purely mechanical (isothermal) models, assuming an instantaneous heat release (see, for example, Făciu and Suliciu, 1994; Vainchtein and Rosakis, 1999), or, in another extreme, purely thermal descriptions, (e.g. Leo et al., 1993), assuming that the motion is controlled by the latent heat removal while phase transformation and stress relaxation are instantaneous. Both approaches, while leading to the important contributions, were only partially successful at explaining the experimentally observed hysteresis loops. Indeed, while the purely mechanical description is able to predict rate-independent hysteresis, the isothermal assumption does not describe the self-heating phenomenon and rate-dependent part of the hysteresis loop. Similarly, the purely thermal models fail to predict the rate-independent part of hysteresis arising due to metastability of equilibria (Vainchtein and Rosakis, 1999).

One of the first models of interface dynamics that included the coupling between the temperature and deformation fields in the non-convex free energy density of an elastic bar was formulated by Abeyaratne and Knowles (1993) in the context of sharp interface theory, which prescribed a *kinetic relation* between interface velocity and the driving force of phase transformation. This relation thus took into account the *internal dissipation* due to phase transition and regularized the problem which is otherwise ill-posed (James, 1980). Additional, thermal, dissipation was also taken into account via the heat conduction mechanism. Abeyaratne and Knowles (1993) also employed a separate *phase nucleation criterion*.

An alternative approach, used in this paper, is to model the internal dissipation by incorporating viscous stresses. This approach has been widely used in the purely mechanical models, both with Kelvin–Voigt viscosity model employed in this model (Ball et al., 1991; Fonseca et al., 1994; Friesecke and McLeod, 1996, 1997;

[1] Throughout this paper, we will refer to hysteresis as being *rate-dependent* (*independent*) if its *size*, defined as the maximum width of a hysteresis loop, does (does not) depend on the loading rate. We remark that other features of a hysteresis loop, such as the amplitude and frequency of serrations, do depend on the loading rate even at a very slow loading. However, the size of the hysteresis does not significantly change under these conditions.

Kalies, 1994; Pego, 1987; Theil, 1998; Truskinovsky, 1994; Vainchtein and Rosakis, 1999) and with Maxwell viscosity (Făciu, 1996a,b; Făciu and Suliciu, 1994). Similarly to the work of Abeyaratne and Knowles (1993), the present model includes a temperature-dependent non-monotone stress–strain law and takes into account inertia, heat conduction and latent heat. Traveling wave solutions for a similar model on an infinite bar have been studied by Ngan and Truskinovsky (1999), who have shown that a *particular* kinetic relation results from including the viscous stresses (see also Truskinovsky, 1994, for the isothermal case). Similar thermodynamic models for the case of *constant* traction or displacement boundary conditions in a finite bar have been studied by Dafermos (1982); Dafermos and Hsiao (1982), Chen and Hoffman (1994) and Jiang (1993), who have shown the global existence of smooth solutions. Racke and Zheng (1997) obtained global existence, uniqueness and the asymptotic behavior of weak solutions to a similar model for the case when both ends of the bar are insulated and at least one end is stress-free. In contrast, our model includes *time-dependent* boundary conditions at the ends of the bar to mimic the tension tests on shape-memory bars and wires. The model results in an initial-boundary value problem containing two strongly coupled non-linear partial differential equations. While mathematically the problem becomes more complex than that of Abeyaratne and Knowles (1993), its advantage is that no additional kinetic relation or nucleation criterion needs to be prescribed. In our model, the motion and formation of interfaces occur after the loading forces the strain to enter the *spinodal region*, or the interval of strains at which the stress decreases, in part of the bar. The spinodal instability then causes an increase in the strain gradient, and phase boundaries start to form, while the system attempts to approach one of the infinitely many multi-phase metastable equilibria. The location and number of boundaries are determined by the viscous and thermal dissipation and the applied strain rate.

A similar approach was independently undertaken by Făciu (2001), who used a Maxwell viscosity in place of the Kelvin–Voigt viscosity model considered here. While the thermomechanical model studied by Făciu (2001) is more complex, including numerous parameters and aiming at the quantitative prediction of the experimental observations, the primary goal of the present work is to qualitatively capture the basic features of the experimental observations and understand the main mechanisms, while keeping the model as simple as possible. This allows us to substantially reduce the number of parameters which makes some analytical work and parameter studies more feasible. Both models are one-dimensional, unlike the plasticity-based three-dimensional model of Shaw (2000). While this has certain disadvantages, in particular inability to predict higher-dimensional phenomena such as criss-cross pattern of interface formation (Shaw and Kyriakides, 1995), it is our hope that a simpler model will shed some more light on the very complex nature of interface dynamics and temperature-deformation coupling.

Another, not viscosity-based, regularization was used by Bubner (1996), who considered a one-dimensional Ginzburg–Landau–Devonshire free energy density, with a strain-gradient term that models interfacial energy, and thermal dissipation in the form of heat conduction. This model is able to predict thermal hysteresis but, unlike the present model, it cannot capture a realistic quasistatic hysteresis because in this case there is a range of end displacements for which there exists only one stable equilibrium, with one phase boundary (Vainchtein and Rosakis, 1999). In addition, the numerical scheme used by Bubner (1996) sometimes yields a mesh-sensitive hysteresis size.

We show that our model is capable of predicting both isothermal and thermal (rate-dependent) portions of hysteresis and the self-heating (self-cooling) effects during loading (unloading). The model also predicts an experimentally observed (Krishnan, 1985) irregular interface motion. Vainchtein and Rosakis (1999) have shown that in the isothermal case (i.e. infinite specific heat) the model results in an alternating stick and slip motion of phase boundaries. In the stick regime, the system followed one of the branches of metastable equilibria with frozen interface locations, while during the slip regime, the spinodal instability resulted in switching from one metastable branch to another, with different interface locations. Phase nucleation, annihilation and interface slip events resulted in *serrated* hysteresis loop which are often observed (Krishnan, 1985; Krishnan and Brown, 1973; Nakanishi, 1975). In this paper, we show that the

stick–slip dynamics is still present at slow loading, small latent heat or high heat conduction. However, faster loading, intermediate heat conduction or higher latent heat all result in the stick–slip dynamics being replaced by the smooth but still irregular, *slow–fast* motion of phase boundaries. This is caused by the inability of the system to remove the heat of transformation quickly enough in order to approach an equilibrium and the resulting competition between the material instability and stabilization due to applied loading. Thus the end-load serrations formerly caused by the stick–slip motion smoothen, and the remaining serrations correspond to nucleation and phase annihilation events. At sufficiently small heat conduction, the smooth interface motion is eventually blocked by the tendency of the system to form multiple boundaries and subsequent stick–slip interface motion and phase annihilation events. Formation of more transformation fronts is also observed at higher loading rates, in qualitative agreement with experimental observations (Shaw and Kyriakides, 1995). By linearizing the problem about an unstable equilibrium and studying the instability growth, we show that multiple nucleation is a result of the dispersion which is especially pronounced at smaller heat conductivity. We show that wider and more inclined hysteresis loops are observed at higher loading rates, in qualitative agreement with experiments (Leo et al., 1993). Finally, we also comment on the effect of viscosity, latent heat and ambient temperature on the interface dynamics.

The structure of this paper is as follows. In Section 2 we introduce the model. In Section 3 we recall some earlier results (Vainchtein and Rosakis, 1999) for the isothermal case. Linear stability analysis of uniform equilibria and the dispersion relation are described in Section 4. The main numerical results and discussion, concentrating on the roles of the main dimensionless parameters, are presented in Section 5. Finally, Section 6 contains summary of the results and concluding remarks.

2. The model

Consider a viscoelastic bar of initial length l_0 and density ρ. Let $x \in [0, l_0]$, $t \in [0, \infty)$ and $u(x,t)$ be the reference coordinate, time and the longitudinal displacement field, respectively. Let $F(u_x, \theta)$ denote the free energy density of the bar, where $u_x(x,t)$ is the strain and $\theta(x,t)$ is the temperature field. Following the approach of Ericksen (1975), we assume that in a certain temperature range, elastic stress

$$\sigma(u_x, \theta) = \partial F / \partial u_x \tag{1}$$

is a non-monotone function of strain u_x, first increasing, then decreasing and increasing again as strain is increased. The intervals of strain in which the elastic stress increases with strain correspond to two different material phases. The strain interval of decreasing stress is called the *spinodal region*. The values of strain at which the *Maxwell line*—a line $\sigma = \sigma_M(\theta)$ that divides the stress–strain graph at fixed θ into two regions with equal areas—intersects the stress–strain curve are called the *Maxwell strains* (see Fig. 1).

The *equilibrium solutions* $(u(x), \theta)$ for such a bar, when it is placed in a hard device (displacement-controlled loading) at temperature θ_0, need to satisfy

$$\begin{cases} \theta = \theta_0 = \text{const.}, & \sigma(u_x, \theta_0) = \text{const.}, \\ u(0) = 0, & u(l_0) = d. \end{cases} \tag{2}$$

Here one end of the bar is fixed, and d denotes the prescribed displacement of the other end. A trivial solution to (2), with uniform strain, is $u(x) = (d/l_0)x$; it is, however, unstable when strain is in the spinodal region. As Ericksen (1975) has shown, an uncountable infinity of other solutions can be constructed. These solutions have continuous displacement $u(x)$ but a piecewise-constant strain $u'(x)$, alternating between two values, say, e_1 and e_2. The finite jump discontinuities in strain can be thought of as phase boundaries. The values $e_{1,2}$ need to be chosen so that

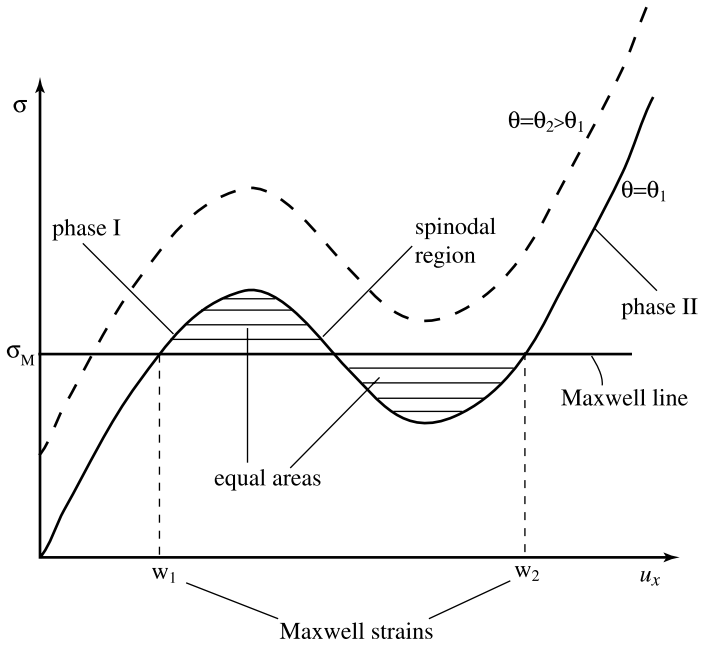

Fig. 1. Non-monotone stress–strain relationship $\sigma(u_x, \theta)$ at fixed temperature.

$$\begin{cases} \sigma(e_1, \theta_0) = \sigma(e_2, \theta_0), \\ se_1 + (1-s)e_2 = d/l_0, \end{cases} \tag{3}$$

where s is the volume fraction of the strain e_1. Then (2) is automatically satisfied. Such solutions are *stable*, in the sense that they are *local* minimizers of energy with respect to smooth variations that *freeze* the locations of interfaces. There are infinitely many of these solutions because, for a given d, only the volume fraction s can be found, while the locations and number of phase boundaries are otherwise completely arbitrary. There is also an infinite number of global energy minimizers, that have strain alternating between the Maxwell strains w_1 and w_2 (see Fig. 1). However, as remarked below, the local minimizers turn out to be more important for the dynamics problem considered here since these are *dynamically stable* (Pego, 1987; Friesecke and McLeod, 1997; Vainchtein and Rosakis, 1999).

To simplify the dynamic analysis, we consider, after Ngan and Truskinovsky (1999), the free energy density

$$F(u_x, \theta) = (K + A\theta)u_x + \mu\left(\frac{1}{4}u_x^4 - \frac{1}{2}u_x^3 + \frac{1}{4}u_x^2\right) - c_e\theta\log\frac{\theta}{\theta_T} + c_e\theta. \tag{4}$$

The elastic stress is then of the form

$$\sigma(u_x, \theta) = K + A\theta + \mu u_x(u_x - 1/2)(u_x - 1). \tag{5}$$

Here we assume that isothermal stress–strain relation is cubic, Maxwell strains $w_1 = 0$ and $w_2 = 1$ are independent of temperature, and Maxwell stress is a linear function of temperature, $\sigma_M(\theta) = K + A\theta$. Parameter μ is twice the elastic modulus at small strains. The specific heat c_e is assumed to be constant. The material constant A controls the latent heat of transformation. When $A > 0$, heat is released when material transforms from the low-strain phase to the high-strain phase, and the Maxwell stress increases with temperature.

Using the above expressions for (4) and (5) for the free energy density and elastic stress, respectively, we obtain the following thermodynamics problem:

$$\begin{cases} \rho u_{tt} = [\sigma(u_x,\theta) + \gamma u_{xt}]_x, \\ c_e\theta_t = \kappa\theta_{xx} + \gamma u_{xt}^2 + A\theta u_{xt}, \\ u(0,t) = 0, \quad u(l_0,t) = d(t), \\ u(x,0) = u_0(x), \quad u_t(x,0) = 0, \\ \theta(0,t) = \theta(l_0,t) = \theta_0, \\ \theta(x,0) = \theta_0. \end{cases} \tag{6}$$

The first and second terms of Eq. (6) express the linear momentum balance and the energy balance, respectively. Here we introduce two different mechanisms of energy dissipation. The first one is the heat conduction, with coefficient of heat conductivity $\kappa > 0$. Another mechanism is the internal dissipation of kinetic origin, modeled by a Kelvin–Voigt viscosity, with coefficient $\gamma > 0$. Note that the boundary conditions (third term of (6)) are *time-dependent*, in an attempt to model the tension experiments on shape-memory-alloy wires, with one end fixed, and another subjected to prescribed displacement. The temperature at the ends equals the ambient temperature θ_0. Initially, the bar is in an equilibrium state $u_0(x)$ at a constant temperature θ_0.

To reduce the number of parameters, we non-dimensionalize the system (6). Choose the length scale l_0 (the initial length of the bar), the stress scale μ (recall (5)), the temperature scale μ/c_e and let the time scale be $l_0\sqrt{\rho}/\sqrt{\mu}$. Without loss of generality, we choose $K = \mu$ (observe that (6) is independent of K). Introducing dimensionless variables

$$\bar{t} = \frac{t\sqrt{\mu}}{l_0\sqrt{\rho}}, \quad \bar{x} = \frac{x}{l_0}, \quad \bar{u} = \frac{u}{l_0}, \quad \bar{\theta} = \frac{\theta c_e}{\mu} \tag{7}$$

and dimensionless parameters

$$\bar{\gamma} = \frac{\gamma}{\sqrt{\mu\rho}l_0}, \quad \bar{A} = \frac{A}{c_e}, \quad \bar{\theta}_0 = \frac{\theta_0 c_e}{\mu}, \quad \bar{\kappa} = \frac{\kappa\sqrt{\rho}}{l_0\sqrt{\mu}c_e}, \quad \bar{d}(\bar{t}) = \frac{d(\bar{t}l_0\sqrt{\rho}/\sqrt{\mu})}{l_0}, \tag{8}$$

we obtain the dimensionless initial-boundary value problem

$$\begin{cases} u_{tt} = [\hat{\sigma}(u_x) + A\theta + \gamma u_{xt}]_x, \\ \theta_t = \kappa\theta_{xx} + \gamma u_{xt}^2 + A\theta u_{xt}, \\ u(0,t) = 0, \quad u(1,t) = d(t), \\ u(x,0) = u_0(x), \quad u_t(x,0) = 0, \\ \theta(0,t) = \theta(1,t) = \theta_0, \\ \theta(x,0) = \theta_0, \end{cases} \tag{9}$$

where all the bars have been dropped and $\hat{\sigma}(w) = 1 + w(w - 1/2)(w - 1)$ represents the dimensionless "temperature-free" part of the elastic stress. We remark on the meaning of the new dimensionless parameters, formerly denoted by barred letters, as in (8). The new γ represents the ratio between time scales due to viscosity (given by

$$\tau_\gamma = \frac{\gamma}{\mu} \tag{10}$$

in original physical variables) and inertia. The new A compares the Clausius–Clapeyron constant (measure of latent heat) to specific heat. Parameter θ_0 is now dimensionless ambient temperature. The non-dimensional κ compares the time scale due to inertia to that arising from heat conduction (given by

$$\tau_\kappa = \frac{c_e l_0^2}{\kappa} \tag{11}$$

in original variables).

We consider the following *loading* program:

$$d(t) = \begin{cases} \dot{\delta}\frac{t^2}{2t_i} + \Delta & \text{for } 0 \leqslant t \leqslant t_i, \\ \dot{\delta}(t - \frac{1}{2}t_i) + \Delta & \text{for } t_i \leqslant t \leqslant t_T - t_i, \\ -\dot{\delta}\frac{(t-t_T)^2}{2t_i} + \Delta_T & \text{for } t_T - t_i \leqslant t \leqslant t_T, \end{cases} \tag{12}$$

with the constant loading rate

$$\dot{\delta} \equiv \frac{\Delta_T - \Delta}{t_T - t_i} \tag{13}$$

except for the initial "impulse" time $0 \leqslant t \leqslant t_i$ and the switch to unloading $t_T - t_i \leqslant t \leqslant t_T$. Here $d(0) = \Delta$ is the initial applied strain (recall that $d(t)$ is now dimensionless and equal to original displacement divided by the initial length), Δ_T is the maximum applied strain, and t_T is the total loading time (see Fig. 2). To study hysteresis, we let the system relax to a high-strain-phase equilibrium (as it is done in experiments), and then *unload* it back to the low-strain phase at the rate $-\dot{\delta}$.

The non-linearity of the problem (9) and the strong coupling between the temperature and displacement fields are better revealed if we express $\theta(x,t)$ in terms of $u(x,t)$ from the first term of (9) (assuming non-zero A):

$$\theta = \frac{1}{A}\left(S(t) - \int_x^1 u_{tt}\,\mathrm{d}y - \hat{\sigma}(u_x) - \gamma u_{xt}\right). \tag{14}$$

Here

$$S(t) = [\hat{\sigma}(u_x(x,t)) + \gamma u_{xt}(x,t)]_{x=1} + A\theta_0 \tag{15}$$

is the *end load* (or effective stress). Substituting (14) in the second term of (9) and employing the boundary and initial conditions in (9), we obtain the following system in terms of displacement field alone:

$$\begin{cases} (\gamma+\kappa)u_{xtt} = \kappa(\hat{\sigma}(u_x))_{xx} + \gamma\kappa u_{xxxt} + u_{xt}\left[A\left(\hat{\sigma}(u_x) + \int_x^1 u_{tt}\,\mathrm{d}y - S(t)\right) - \hat{\sigma}'(u_x)\right] + S'(t) - \int_x^1 u_{ttt}\,\mathrm{d}y, \\ u(0,t) = 0, \quad u(1,t) = d(t), \quad \int_0^1 u_{tt}\,\mathrm{d}y = [\hat{\sigma}(u_x) + \gamma u_{xt}]_{x=0}^{x=1}, \\ u(x,0) = u_0(x), \quad u_t(x,0) = 0, \quad u_{tt}(x,0) = (\hat{\sigma}(u_0'(x)))_x. \end{cases} \tag{16}$$

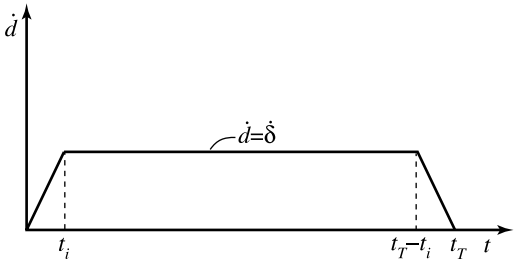

Fig. 2. Loading rate.

The first term of Eq. (16) is nonlocal (due to inertia) and highly nonlinear. When the strain $w(x,t) = u_x(x,t)$ is in one of the phases, it is a nonlinear wave equation for w, with two damping terms: a linear term $\gamma\kappa w_{xxt}$ and a nonlinear (and generally nonlocal) term

$$w_t\left[A\left(\hat{\sigma}(w) + \int_x^1 u_{tt}\,\mathrm{d}y - S(t)\right) - \hat{\sigma}'(w)\right].$$

The nonlinear damped wave equation arises due to heat conduction and the strong coupling between the temperature and deformation fields, and it persists even when the inertia term is neglected. We will come back to this point later.

3. Isothermal case: serrated loops and stick–slip motion

In this section we briefly recall some earlier results for the isothermal case in which the heat is assumed to be removed instantaneously (infinite specific heat c_e in (6)) and the temperature is constant in the bar. The problem then reduces to a purely mechanical description. It was considered by Vainchtein and Rosakis (1999), for the case of symmetric boundary conditions and the cubic stress–strain relation $\sigma(u_x) = u_x^3 - u_x$:

$$\begin{cases} \rho u_{tt} = [\sigma(u_x) + \gamma u_{xt}]_x, \\ u(0,t) = -d(t), \quad u(1,t) = d(t), \\ u(x,0) = u_0(x), \quad u_t(x,0) = 0. \end{cases} \tag{17}$$

The results are summarized in Fig. 3. Initially, the material was in the low-strain phase, with uniform strain $u_x = -1$. As the loading was applied, the strain in the bar increased, and eventually entered the spinodal region. The spinodal instability then led to the formation of several interfaces (two in the simulation shown here). Afterward, the phase boundaries underwent an irregular *stick–slip* motion, a series of alternating quasistatic (stick) and dynamic (slip) events. During the *stick* regime, the system followed rather closely one of the quasistatic solution branches (shown by the dashed lines in Fig. 3) with fixed volume fraction s of the low-strain phase, motionless sharp interfaces and increasing average strain. After the strain in a portion of the bar entered the spinodal region, the *slip* event occurred, and the old strain discontinuities (interfaces) were smoothened and replaced by the new ones at different locations, thus approaching another quasistatic branch, with smaller s. More details can be found in Vainchtein and Rosakis (1999). The hysteresis loops

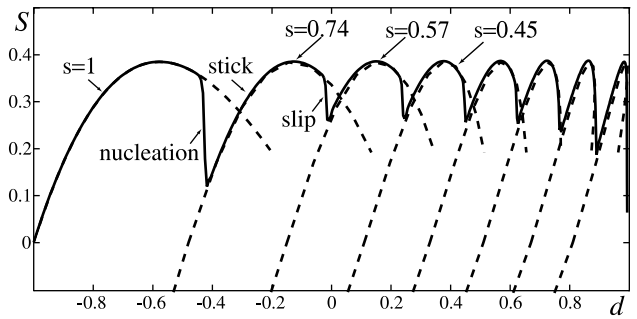

Fig. 3. The results of simulation for the isothermal model (17) with $\rho = 0.05$, $\gamma = 0.1$, $t_T = 100$, $t_i = 0.01$. The thick solid line gives the load (S) versus elongation (d) for the dynamic solution. The dashed lines correspond to analytically computed quasistatic solution branches. The volume fraction s of the low-strain phase is fixed along each branch. Only the quasistatic branches followed by the dynamic solution during the stick regime are shown. The drops in S for the dynamic solution correspond to the nucleation (first drop) and slip events. From Vainchtein and Rosakis (1999).

obtained in the isothermal case are thus serrated, and the interfaces move irregularly, in qualitative agreement with some quasistatic experiments in single-crystal shape-memory alloys (Krishnan, 1985). Similar results have been also obtained by Făciu and Suliciu (1994) for a Maxwell rate-type viscosity model in place of the Kelvin–Voigt model studied here.

The important conclusion following from these studies is that the *isothermal* (quasistatic, rate-independent) portion of the hysteresis is primarily due to the material getting locked in the metastable equilibrium branches. At slow loading, the viscous effects are rather minor, and do not significantly contribute to hysteresis. In contrast to the purely thermal descriptions (Leo et al., 1993), where the size of isothermal hysteresis, σ_{hyst}, had to be postulated, the purely mechanical models mentioned here are able to *predict* σ_{hyst} and its origin.

What these models *cannot* predict, unlike Leo et al., 1993), is the thermally induced, rate-dependent portion of the hysteresis, as well as other thermal effects, such as self-heating (self-cooling) during loading (unloading). As we shall see below, the model considered in the present paper is able to predict both isothermal hysteresis and thermal effects.

4. Dispersion relation

We now return to the full thermodynamics description (9). Before we describe the numerical solution to (9), it is useful to take a look at the linear stability of equilibrium solutions with uniform strain and constant temperature, at constant end displacement $d(t) = d_0$. With this in mind, we linearize (16) about such an equilibrium $(d_0 x, \theta_0)$. We then obtain the following eigenvalue problem for the perturbation $\eta(x,t)$ from the equilibrium displacement:

$$\begin{cases} (\gamma+\kappa)\eta_{xtt} = \kappa\xi\eta_{xxx} + \gamma\kappa\eta_{xxxt} - (\lambda+\xi)\eta_{xt} - \int_x^1 \eta_{ttt}\,\mathrm{d}y, \\ \eta(0,t) = \eta(1,t) = 0, \quad \int_0^1 \eta_{tt}\,\mathrm{d}y = [\xi\eta_x + \gamma\eta_{xt}]_{x=0}^{x=1}. \end{cases} \tag{18}$$

Here $\xi = \hat{\sigma}'(d_0)$ is a local elastic modulus when positive and a measure of material instability when negative (i.e. when linearization is about the strain in spinodal region), and $\lambda = A^2\theta_0$ is the measure of latent heat. Seeking the perturbation in the form of sine Fourier series

$$\eta(x,t) = \sum_{\text{even } n} A_n \mathrm{e}^{\omega t} \sin(\pi n x) \tag{19}$$

(the sum is over even n so that the boundary conditions (18, second term) are satisfied), we arrive at the following *dispersion relation*:

$$\omega^3 + (\kappa+\gamma)\omega^2(\pi n)^2 + \omega[(\lambda+\xi)(\pi n)^2 + \kappa\gamma(\pi n)^4] + \kappa\xi(\pi n)^4 = 0. \tag{20}$$

This cubic equation has three roots. If ξ is positive, the real parts of all three roots are negative, thus implying linear stability of states in either of the phases (Ngan and Truskinovsky, 1999). When we linearize about the state with strain in spinodal region, $\xi = \hat{\sigma}'(d_0)$ is negative, and one of the three roots of (20) is real and positive, thus causing exponential growth of perturbations and *material instability*. It can be shown that this is also the only root with positive real part.

Let ω_n be the rate of instability growth. Fig. 4 shows the effect of the three main dimensionless parameters, κ, λ and γ, on the resulting dispersion curves. Two special cases need to be considered. In the first, *isothermal*, case, both κ and λ vanish (infinite specific heat), and the dispersion curve is shown by a thick line in Fig. 4a. In the second, *adiabatic*, case, only κ vanishes (zero heat conductivity), and the dispersion curve is shown by a dashed line in Fig. 4a. As in the purely mechanical model (Vainchtein and Rosakis, 1999),

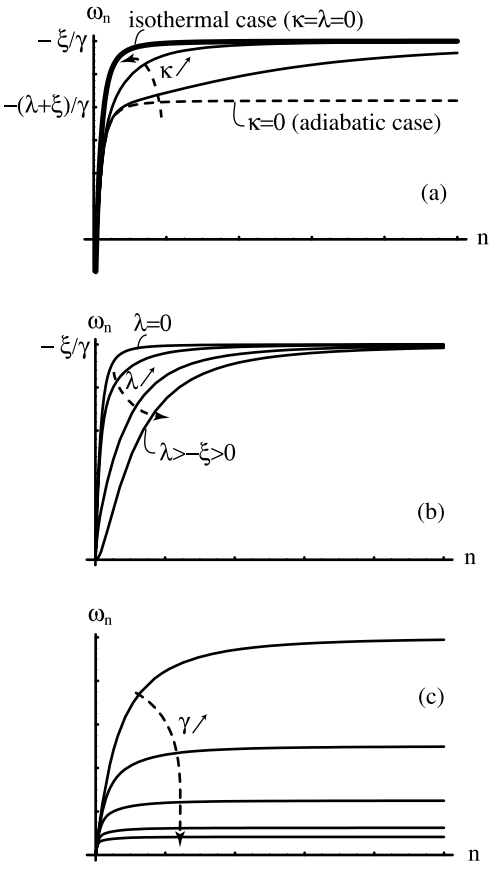

Fig. 4. The effect of (a) heat conductivity κ, (b) measure of latent heat λ, (c) viscosity γ on the rate of instability growth ω_n.

both curves show some dispersion due to inertia. In each case, as n tends to infinity, ω_n tends to a constant given by $-(\lambda+\xi)/\gamma$. Notice that the limit is lower in the adiabatic case due to the presence of latent heat measured by $\lambda > 0$. No instability is observed in the adiabatic case if $\lambda + \xi > 0$ (positive adiabatic sound speed) even if linearization is about the state with strain in the spinodal region ($\xi < 0$).

Now consider a general heat-conductive material. In this case a dispersion curve is close to the adiabatic one (with the same initial slope, $\pi\sqrt{-(\lambda+\xi)}$, if $\lambda+\xi$ is negative, and zero otherwise), but approaches the isothermal curve at large mode numbers n (see Fig. 4a). This behavior creates an *additional dispersion* due to heat conduction which persists even if inertia term is neglected. This dispersion is especially pronounced at small κ. Since the initial slope is controlled by the latent heat, as shown in Fig. 4b, the low modes grow *slower* than in the isothermal case.

It can be shown that, for a given initial perturbation, only a *finite* range of modes will be amplified the most, with the maximum number $n_{\max}$ higher at smaller (non-zero) heat conductivity κ due to the additional dispersion. Similarly to the isothermal case (Vainchtein and Rosakis, 1999), the maximum number of amplified modes also increases as the viscosity γ is decreased (see Fig. 4c for the effect of viscosity on ω_n). In nonlinear regime, these instabilities lead to formation of interfaces. Thus, we can expect to see more phase boundaries forming at smaller non-zero κ and smaller γ.

5. Thermodynamics: numerical results and discussion

In this section we describe the numerical solutions of (9), concentrating on the effect of the main dimensionless parameters: heat conductivity κ, latent heat constant A, ambient temperature θ_0, viscosity γ and loading rate $\dot{\delta}$. We have used the following semi-implicit finite-difference algorithm to approximate (9). At each time-step, the displacement field was calculated first. Here we adapted the scheme of Swart (1991) to solve the first term of (9), which uses the central-difference approximation for the acceleration term u_{tt}, the implicit Euler method for the viscosity term γu_{xt} and incorporates the explicit conservation-form approximation of the nonlinear term. Once the displacement was updated, temperature was calculated using the implicit Crank–Nicolson method to approximate the energy balance (second term (9)). Convergence of the numerical method was checked by reducing the mesh sizes in both space and time, and no mesh dependence was found in the results presented below.

5.1. Effect of κ

We start with the effect of dimensionless heat conductivity κ. The numerical results are summarized in Fig. 5. In all simulations presented in this paper, the bar is initially in the low-strain-phase equilibrium. The applied loading, combined with the fixed-temperature boundary conditions (fifth term (9)), creates the temperature gradient (concave temperature profile) which, in turn, creates a strain gradient (convex strain profile). Thus the strain at the ends of the bar enters the spinodal region first, and two phase boundaries are formed. As κ is decreased, this first interface formation occurs *sooner* because the bar is heated up more by the loading, which results in a higher strain gradient.

When κ is large (see the case $\kappa = 100$ in Fig. 5), the material behavior is almost isothermal: like in the isothermal case, the system undergoes a series of nucleations and then stick–slip interface motion, with the heat generated by transformation quickly removed during the nucleation, slip and annihilation events. See also Fig. 6. Except for these dynamic events, the temperature field is almost uniform, and in each of the stick regimes the system is close to an equilibrium.

Observe that during the nucleation and slip events the temperature in the low-strain portion of the bar first drops and then increases. For example, during the first nucleation, shown in Fig. 6c, d, the temperature in the middle of the bar decreases between $t = 40$ and 42 and then increases until the second nucleation takes place shortly before $t = 43$. Similar initial decreases in temperature during nucleation were also observed by Bubner (1996). To explain this phenomenon, recall the second term of Eq. (9) for the temperature evolution. Prior to the first nucleation event, the temperature profile in the bar was concave due to the boundary conditions and the applied loading (see above), thus $\kappa\theta_{xx} < 0$ initially. After the strain gets sufficiently far in the spinodal region, the instability forces the strain in the middle of the bar to decrease, so that the strain rate, and hence the last term in the right-hand side of second term of (9), are negative: $A\theta u_{xt} < 0$. The second term, γu_{xt}^2, is positive, but at non-zero A and sufficiently small u_{xt} it is smaller than the magnitude of the third term. Thus, for a short time, the combination of the first and third negative terms forces the temperature to decrease. Of course, the decrease in temperature eventually makes its profile locally convex, thus changing the sign of the first term to positive, and, as the amplitude of u_{xt} becomes large enough, the second term dominates and the overall temperature rate becomes positive again. We note that while the temperature may slightly decrease prior to self-heating in experiments, the cooling observed here (e.g. $\theta < \theta_0$ at $t = 42$ and 58 in Fig. 6d, f) seems unrealistically severe. We note, however, that at lower heat conductivity or higher loading rates, self-heating is much more prevalent during loading than self-cooling, as we shall see below. In addition, taking convection into account would prevent the temperature from dropping below θ_0 in the simulation considered above.

As we reduce κ, the time it takes for the system to remove the heat, which is generated by the transformation and constantly supplied by the loading, increases (recall that time scale introduced by the heat

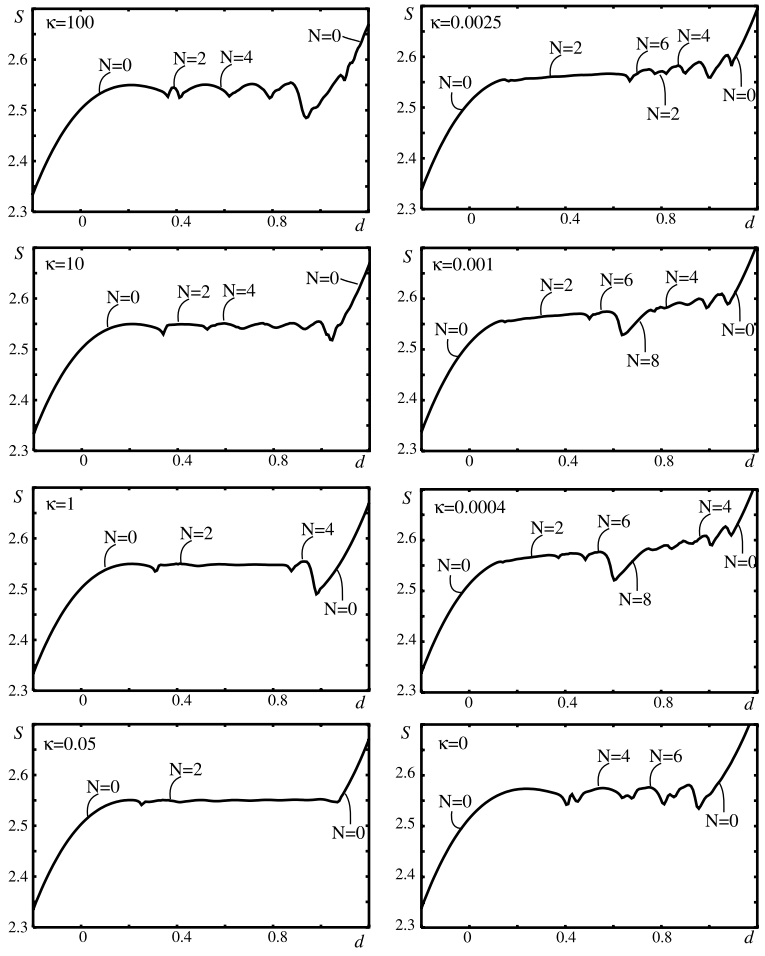

Fig. 5. The effect of heat conductivity κ on the end load versus elongation curve $S(d)$ during loading: $\gamma = 0.1$, $A = 0.03$, $\theta_0 = 50$, $t_i = 0.01$, $\dot{\delta} = 0.016$. The number of phase boundaries is denoted by N.

conduction is given by (11)). A representative picture for the intermediate values of κ is shown in Fig. 7. Unlike the isothermal and almost isothermal (large κ) cases, the strain profiles are rather smooth in this case, especially near the low-strain-phase portion. Following the first nucleation event ($t = 38$ to 41 in Fig. 7c), the interfaces attempt to slow down (while the strain profile *sharpens*) to the equilibrium locations, but, due to the presence of the temperature gradient, are unable to do so quickly enough before the increasing applied strain carries a large portion of the bar in the spinodal region ($t = 41$). The spinodal instability then increases the strain gradients in this portion and *smoothens* the strain profile (thus quickly "moving" the interfaces), a behavior typical during a slip event ($t = 41$ to 45). Afterward, the system again attempts to sharpen the strain profile, and the interfaces slow down ($t = 45$ to 50 in Fig. 7e), before a large portion of the bar again has strain in the spinodal region and the smoothening takes place ($t = 50$ to 54) etc. In contrast to the stick–slip interface dynamics observed above, the phase boundaries now move in an irregular, slowing-down–speeding-up fashion (one can say that only dynamic slip events are now observed). This is caused by the *competition* between spinodal instability (which, in the absence of time-dependent loading, would cause relaxation to a sharp-interface equilibrium) and the stabilization due to loading which

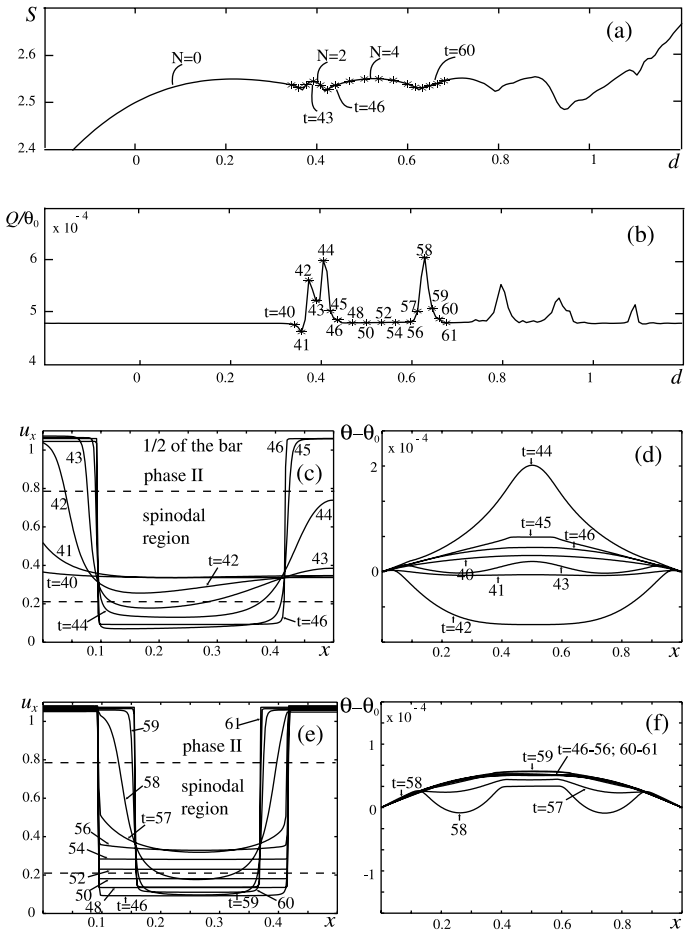

Fig. 6. Solutions at $\kappa = 100$: (a) end load versus elongation $S(d)$; (b) released heat $Q = -\kappa\theta_x|_{x=0}^{x=1}$, normalized by the initial and end temperature θ_0, versus d; (c) strain and (d) temperature profiles during nucleation: $t = 40$ to 46; (e) strain and (f) temperature profiles during first stick–slip motion event: $t = 46$ to 59. Due to symmetry of solutions, only half of the bar is shown in the strain profiles.

is aided by the inability of the system to remove the heat quickly enough. Eventually, the two interfaces move close enough to each other for the phase annihilation to take place, so that the whole bar is transformed to the high-strain phase.

Thus, as κ is decreased to the intermediate values, the serrations previously caused by the stick–slip dynamics, smoothen out. The interface motion is now smooth (although irregular), and the only true serrations are caused by the nucleation and phase annihilation events. Such behavior is observed in tension experiments on polycrystalline shape-memory wires conducted in air (Leo et al., 1993; Shaw and Kyriakides, 1995).

As we decrease κ to much smaller values, the nucleation of a pair of interfaces and their irregular motion initially take place, but eventually the smooth interface motion is stopped by the tendency of the system to form multiple boundaries. This is caused by the *additional dispersion* mentioned above in the linear stability analysis of Section 4. The dispersion is especially pronounced at small (but non-zero) values of κ. Recall that with non-zero latent heat, the modes grow slower as κ decreases. It can also be shown that the number of instability modes amplified the most increases with the length of the portion of the bar inside the

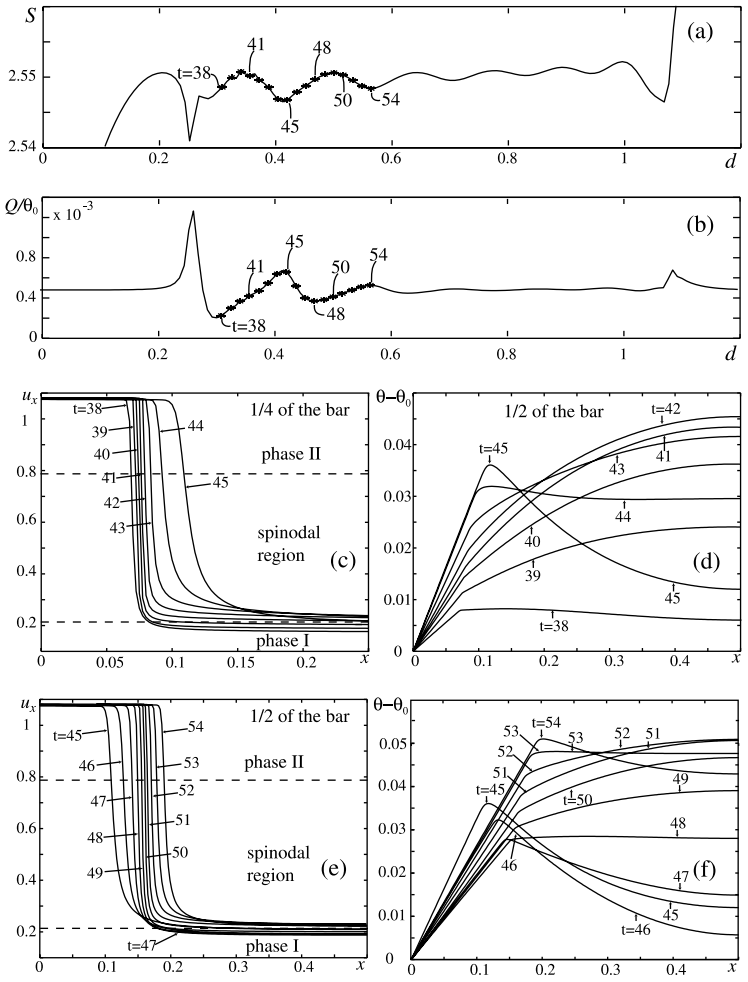

Fig. 7. Solutions at $\kappa = 0.05$: (a) end load versus elongation $S(d)$; (b) ratio of released heat to initial temperature, Q/θ_0, versus d; (c) strain (quarter of the bar) and (d) temperature (half of the bar) profiles during the time interval $t = 38$ to 45; (e) strain and (f) temperature profiles (half of the bar) during the time interval $t = 45$ to 54.

spinodal region. Thus the nucleation of multiple interfaces does not occur until a substantial portion of the bar has strain in spinodal region. As Fig. 5 shows, up to eight boundaries form altogether at $\kappa = 0.0004$, as opposed to four in the almost isothermal case $\kappa = 100$. After the nucleation takes place, the severe instability *sharpens* the interfaces (recall that the growth rate ω_n for linear instability is much higher at higher instability mode numbers n; the growth rate also increases as the strain gets deeper in the spinodal region), so that the strain profile is now piecewise-smooth. See the case of $\kappa = 0.0025$ (Fig. 8), in which the formation of six sharp interfaces takes place at $t = 63$. Following the formation of multiple interfaces ($t \geqslant 63$ in Fig. 8e), stick–slip interface motion and nucleation and annihilation events are observed, accompanied by serrations in the end load. No smooth interface motion occurs after the sharp interfaces have been formed.

Thus at small κ two types of interface motion are observed: the smooth irregular slow–fast motion following the first nucleation, and the stick–slip motion after additional boundaries have been formed. As κ

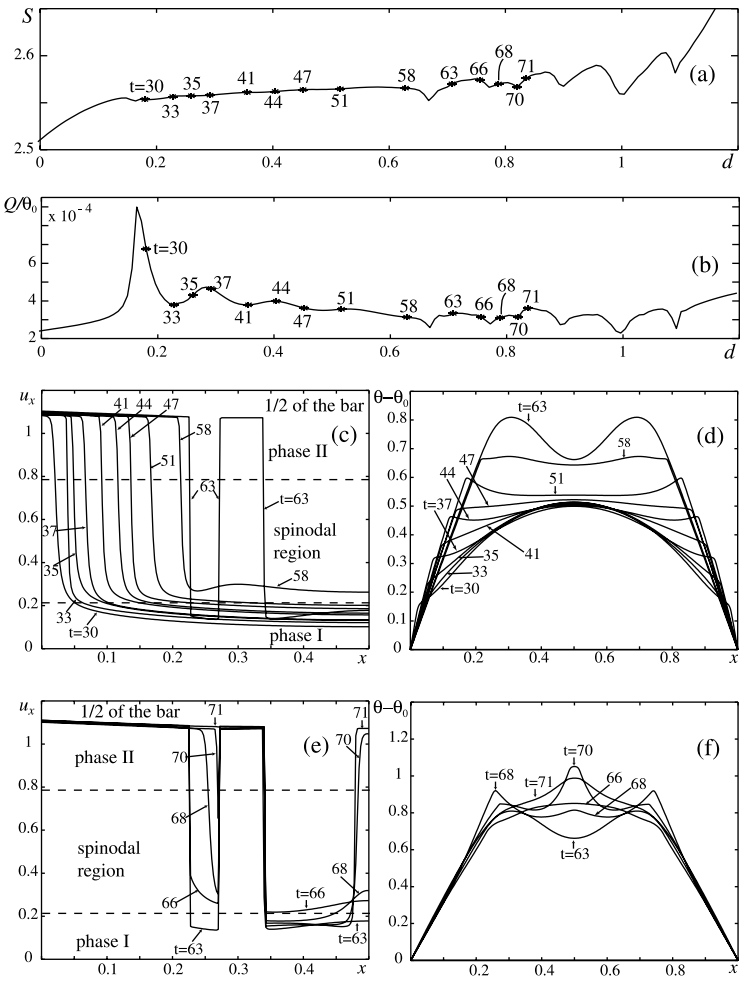

Fig. 8. Solutions at $\kappa = 0.0025$: (a) end load versus elongation $S(d)$; (b) ratio of released heat to initial temperature, Q/θ_0, versus d; (c) strain and (d) temperature profiles prior to the multiple interface formation: $t = 30$ to 63; (e) strain and (f) temperature profiles during the stick–slip interface motion following the multiple interface formation: $t = 63$ to 71. Due to symmetry of solutions, only half of the bar is shown in the strain profiles.

decreases, less and less of the load–elongation curve corresponds to the smooth interface motion, with the severe *self-heating* of the bar (see the temperature profiles in Figs. 8d,f) speeding up the nucleation process. The heating of the bar at smaller κ also creates an overall positive slope of the load–elongation curve, commonly observed in experiments conducted under more adiabatic loading conditions (Leo et al., 1993; Shaw and Kyriakides, 1995) (at higher loading rates and in a less convective medium, such as air).

Finally, in the adiabatic case, $\kappa = 0$, no smooth interface motion is observed, and there are serrations due to nucleation and annihilation events and stick–slip interface dynamics. This case is rather special, because the fixed-temperature boundary conditions (fifth term of (9)) are now irrelevant. Thus, unlike the case with non-zero κ, no significant temperature gradient is created during loading in the low-strain phase, and both strain and temperature increase in time and are nearly uniform in space (some gradient is caused by inertia) until the first instability occurs. Recall from the linear stability analysis (Section 4) of the

uniform-strain equilibria, with strain w and temperature θ, that in the adiabatic case the instability condition is that the *adiabatic sound speed* $c_a = \lambda + \xi = A^2\theta + \hat{\sigma}'(w)$ must vanish. Much like in the isothermal case, nucleation does not take place until the *whole bar* has strain sufficiently deep in the spinodal region so that the *adiabatic* speed c_a (as opposed to the isothermal speed $c = \hat{\sigma}'(w) = \xi$ in the isothermal case) becomes negative. This is why the first nucleation occurs much later than in non-zero-κ cases, where the temperature, and hence strain, gradients make it possible for nucleation to occur after only a *portion* of the bar has strain in the spinodal region. After the nucleation, the temperature profile is no longer continuous in the adiabatic case.

Observe that during the irregular interface motion at the intermediate values of κ, both released heat and the end load (as well as strain and temperature fields) undergo damped oscillations in time (or as functions of applied strain d). See Fig. 7. This can be explained if we recall the first term of Eq. (16) derived above for the displacement field alone. As mentioned above, when strain is in either of the phase regions, this equation describes damped nonlinear (and nonlocal) waves in strain. While there certainly are inertia waves damped by viscosity (which are also captured by the simulations and are distinctly more visible as viscosity is decreased—see Section 5.3), the waves observed here are primarily due the heat conduction. To show this, we neglect the inertia terms in (16, first term) and arrive at

$$\gamma w_{tt} = \kappa(\hat{\sigma}(w))_{xx} + \gamma\kappa w_{xxt} + w_t[A(\hat{\sigma}(w) - S(t)) - \hat{\sigma}'(w)] + S'(t), \tag{21}$$

where $w(x,t) = u_x(x,t)$ is the strain field. One can see that, even though the inertia term has been neglected, the nonlinear oscillations persist for general (intermediate) values of κ. As before, there are two damping terms, linear viscosity-like damping $\gamma\kappa w_{xxt}$ and nonlinear damping term $w_t[A(\hat{\sigma}(w) - S(t)) - \hat{\sigma}'(w)]$. As κ tends to infinity, Eq. (21) reduces to $\gamma w_{xxt} = (\hat{\sigma}(w))_{xx}$, and the oscillations (in the absence of inertia) disappear. Similarly, there are no oscillations (not due to inertia) when $\kappa = 0$. But at the intermediate values of κ, one can expect damped oscillations of strain (and thus, via (14), temperature) due to heat conduction.

5.2. Effect of A and θ_0

Parameter A controls the amount of latent heat and thus measures the coupling between the temperature and deformation fields. As Fig. 9 shows, when A is sufficiently small (e.g. $A = 0.0003$, $A = 0.003$), the two fields are very weakly coupled, and thus the problem is almost purely mechanical, as in the isothermal case. Thus, we observe behavior similar to that of the isothermal model (Vainchtein and Rosakis, 1999). In this case, up to four interfaces form and then propagate in a stick–slip manner. As we increase A, the first nucleation occurs sooner, since the temperature gradient caused by the loading induces a more substantial strain gradient at higher A. Naturally, the load–elongation curve shifts up as A is increased, in view of (5), but only the "temperature-free" portion of the end load, $S–A\theta_0$, is shown in Fig. 9.

When A becomes sufficiently high (e.g. $A = 0.01$ in Fig. 9), the slow–fast interface motion described above is observed. The amplitude of end-load oscillations decreases as A grows. Overall, the latent heat has a stabilizing effect on the transformation: as A increases, fewer boundaries are formed (only two at $A = 0.6$ versus four at small A) and the strain profile smoothens. Recall from the analysis of Section 4 that latent heat slows down the growth of instabilities. Incidentally, in the *adiabatic case* $\kappa = 0$ no instability takes place at $A = 0.6$, since the adiabatic sound speed is always positive when latent heat is sufficiently high, while in the non-zero-κ case the temperature-induced instability occurs when strain enters the spinodal region (isothermal sound speed vanishes). Observe also the increasing overall slope of the load–elongation curve as A grows.

The effect of dimensionless ambient temperature, θ_0, is shown in Fig. 10. In addition to shifting the end-load curve up by $A\theta_0$, increasing ambient temperature also increases the overall heating of the bar during loading, thus resulting in a wider thermal hysteresis. Similar to the latent heat constant A, higher initial

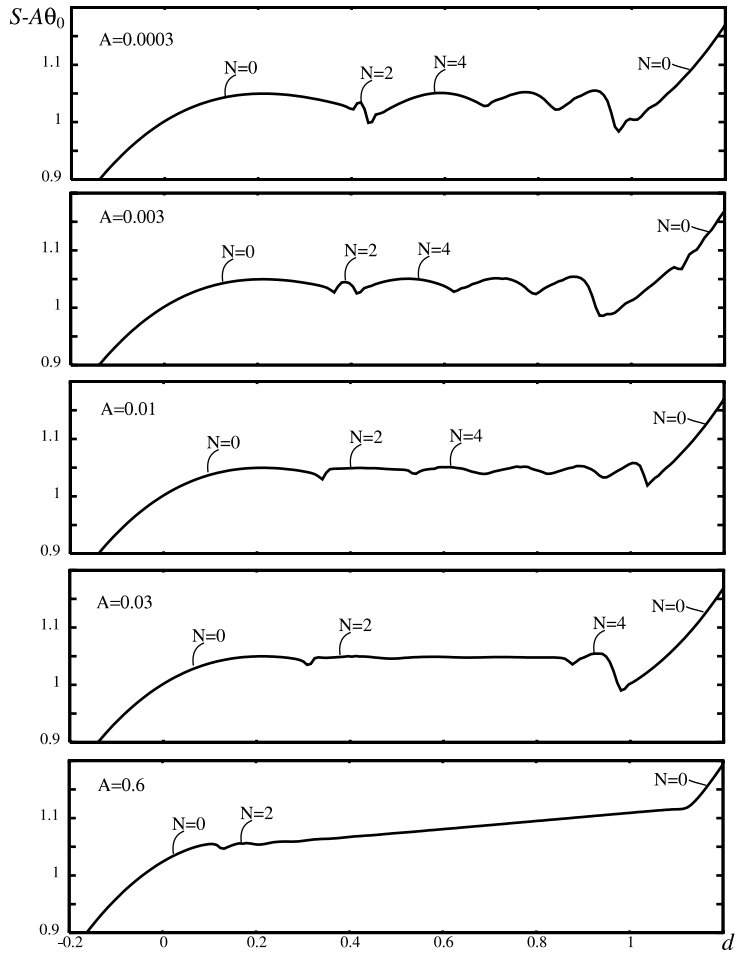

Fig. 9. The effect of the parameter A on the "temperature-free" part of the end load versus elongation curve $S(d)$–$A\theta_0$ during loading: $\gamma = 0.1$, $\kappa = 1$, $\theta_0 = 50$, $t_i = 0.01$, $\dot{\delta} = 0.016$.

temperature results in the earlier first nucleation. The period and amplitude of the end-load oscillations do not seem to be affected much by the value of θ_0.

5.3. Effect of γ

The effect of the third parameter, dimensionless viscosity γ, at the intermediate value of the heat conduction, $\kappa = 0.05$, is shown in Fig. 11. At smaller γ (dashed and solid curves) the figure clearly shows two kinds of oscillations in both end load and released heat. The higher-frequency oscillations are the usual damped sound waves, and these are much more pronounced at smaller γ. The lower-frequency oscillations correspond to the damped oscillations mentioned above that are primarily due to heat conduction. These oscillations are actually damped more as γ is decreased, since the "inertia" term for these oscillations (recall first term of (16), (21)) decreases as γ is decreased. In general, lower viscosity leads to higher instability growth rate (recall Fig. 4c) and thus shortens the time needed for interface sharpening and nucleation.

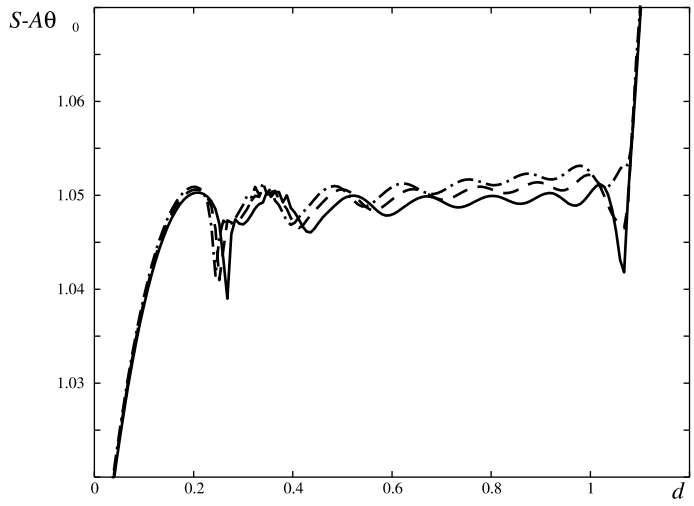

Fig. 10. The effect of dimensionless ambient temperature θ_0 on the "temperature-free" part of the end load versus elongation curve $S(d)$–$A\theta_0$ during loading: $\gamma = 0.1$, $\kappa = 0.05$, $A = 0.03$, $t_i = 0.01$, $\dot{\delta} = 0.016$. Solid curve: $\theta_0 = 30$, dashed curve: $\theta_0 = 50$, dash-dotted curve: $\theta_0 = 70$.

5.4. The effect of the loading rate on hysteresis

Finally, we remark on the effect of the loading rate on the size and other features of the hysteresis loops for our model. See Fig. 12. At slow loading ($\dot{\delta} = 0.0016$) only two interfaces are formed, and these move in the stick–slip fashion during virtually isothermal phase transformation. Thus, unlike the model of Leo et al. (1993), the present model predicts the *isothermal* hysteresis observed at quasistatic loading.

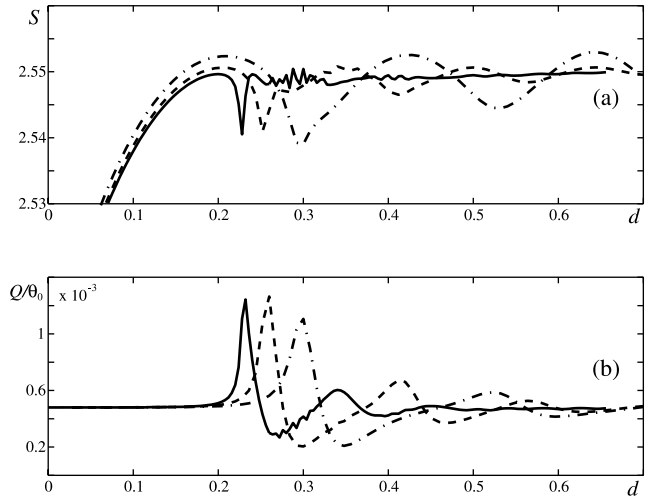

Fig. 11. The effect of the parameter γ on the (a) end load versus elongation curve $S(d)$, (b) the ratio released heat to initial temperature, Q/θ_0, during loading. Solid curve: $\gamma = 0.05$, dashed curve: $\gamma = 0.1$, dash-dotted curve: $\gamma = 0.2$. Other parameters: $\kappa = 0.05$, $\theta_0 = 50$, $A = 0.03$, $t_i = 0.01$, $\dot{\delta} = 0.016$.

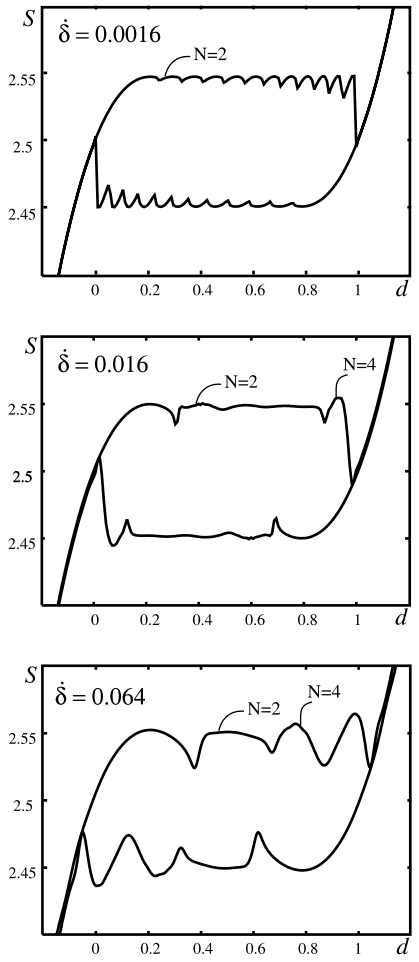

Fig. 12. The effect of the dimensionless loading rate $\dot{\delta}$ on formation and motion of phase boundaries: $\kappa = 1$, $\gamma = 0.1$, $\theta_0 = 50$, $A = 0.03$, $t_i = 0.01$.

As the loading rate is increased ($\dot{\delta} = 0.016$), more interfaces are formed (up to four), since the thermal effects induce instability. The serrations formerly caused by the stick–slip motion smoothen, while the interfaces move in an irregular slow–fast fashion, as described above. At even higher loading rate ($\dot{\delta} = 0.016$) there are more pronounced oscillations in end load, due to viscous stabilization (which delays the nucleation of the first two-phase boundaries at higher loading rates), but the interface motion is smooth and not stick–slip. Notice that the two additional interfaces are formed earlier at the higher $\dot{\delta}$, due to the higher temperature gradient.

The size of the hysteresis (defined as the maximum width of the loop) increases with the loading rate, as shown in Fig. 13. Part of the increase is due to the viscous effects but the main contribution is from the thermal effects. Observe that the overall slope of the loops also increases, due to a more substantial heating (cooling) of the bar during loading (unloading) at higher rates. Both of these observations, as well as formation of more interfaces at higher loading rates, are in qualitative agreement with experiments (Leo et al., 1993).

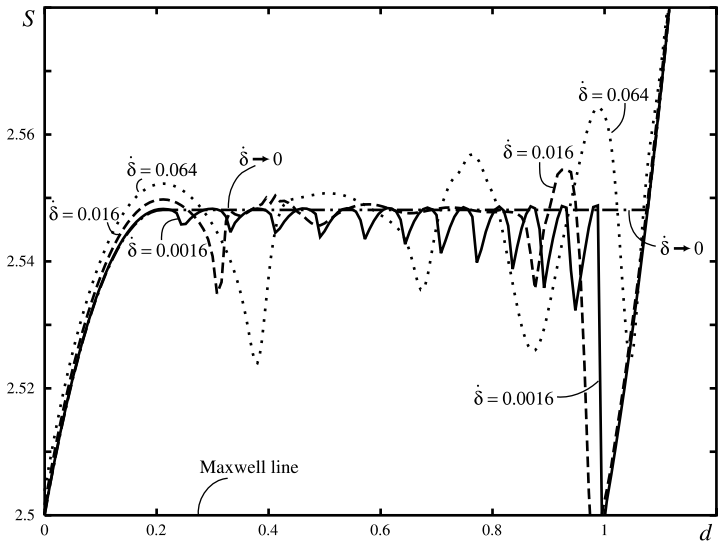

Fig. 13. The effect of $\dot{\delta}$ on the size and overall slope of the hysteresis loops: $\kappa = 1$, $\gamma = 0.1$, $\theta_0 = 50$, $A = 0.03$, $t_i = 0.01$. Only upper halves of the hysteresis loops (above the Maxwell line) are shown. Dash-dotted line depicts the quasistatic (isothermal) hysteresis as predicted by Vainchtein and Rosakis (1999).

6. Summary and concluding remarks

In this paper we considered a thermomechanical model of martensitic phase transitions in thin bars and wires. While intentionally simplified, the model includes both nonlinearly elastic mechanical description, with inertia and internal dissipation via viscous stresses, and thermal dissipation in the form of heat conduction. The model also incorporates in the simplest way the strong coupling between temperature and deformation fields, thus taking latent heat of transformation into account. In this first, exploratory study of the model we have focused on the role of the primary dimensionless parameters. The main conclusions are:

- The model is capable of predicting both rate-independent *isothermal hysteresis* at quasistatic loading and additional, *rate-dependent hysteresis* due to thermal effects.
- At high heat conductivity the behavior of the system is "almost isothermal": similarly to the isothermal case, interfaces move in a *stick–slip* fashion, and the heat is quickly removed during nucleation and slip events. Such non-smooth interface motion is also present in case of small latent heat, i.e. when the coupling between temperature and deformation fields is weak, and at sufficiently slow applied loading. The resulting hysteresis loops are serrated.
- At intermediate values of heat conductivity (or larger latent heat) and faster loading, the stick–slip motion is partially replaced by a smooth, yet irregular, *slow–fast* interface motion accompanied by damped oscillations in the end load and released heat. These nonlinear oscillations are due to heat conduction and persist even when inertia is neglected. Their period and amplitude also depend on the viscosity coefficient and the loading rate.
- At sufficiently small heat conductivity, the smooth propagation of phase boundaries is eventually blocked by formation of multiple interfaces caused by a dispersion in the instability growth rate. After these additional boundaries have formed, stick–slip interface motion takes place. In the *adiabatic* case (zero heat conduction) only stick–slip motion is observed.

- As the applied loading rate is increased, *self-heating* (self-cooling) of the bar during loading (unloading) are observed and more interfaces are formed. These thermal effects lead to the increasing hysteresis size. Wider loops are also observed at higher latent heat and ambient temperature.
- The linearization about an unstable uniform-strain equilibrium and the effect of latent heat, viscosity and heat conductivity on the growth rate of instabilities were also discussed. In particular, the analysis reveals the connection between the special isothermal and adiabatic cases and the general case of heat-conducting material.

The numerical experiments presented here clarify the role of heat conduction, viscosity, latent heat and loading rate on the size and qualitative features of the hysteresis loop and the dynamics of interface propagation. We hope that the simplified model considered here will allow us to carry out more analytical work to confirm some of these predictions. In particular, further simplifications, such as study of traveling wave solutions and the case with neglected inertia term and trilinear, rather than fully nonlinear, material may be useful. In addition, simulations of inner loops (unloading the bar before the complete transformation has occurred and reloading) are currently under way.

In order to conduct a quantitative comparison with experiments, however, one must consider a more sophisticated model. In particular, such a model should include convective heat exchange with the surrounding medium, in order to explain the difference in the hysteresis size in experiments conducted in water and air (Leo et al., 1993), and the dependence of Maxwell strains on temperature. It should also take into account the fact that austenite and martensite have different thermal properties. The situation is further complicated by the lack of experimental data in the spirit of Leo et al. (1993) and Shaw and Kyriakides (1995) for single-crystal shape-memory-alloy wires, for which the present model is relevant.

References

Abeyaratne, R., Knowles, J., 1993. A continuum model of a thermoelastic solid capable of undergoing phase transitions. Journal of the Mechanics and Physics of Solids 41, 541–571.

Ball, J., Holmes, P., James, R., Pego, R., Swart, P., 1991. On the dynamics of fine structure. Journal of Nonlinear Science 1, 17–70.

Bubner, N., 1996. Landau–Ginzburg model for a deformation-driven experiment on shape memory alloys. Continuum Mechanics and Thermodynamics 8, 293–308.

Chen, Z., Hoffman, K.-H., 1994. On a one-dimensional nonlinear thermoviscoelastic model for structural phase transitions in shape memory alloys. Journal of Differential Equations 112, 325–350.

Chu, C., 1993. Hysteresis and microstructures: a study of biaxial loading on compound twins of copper–aluminum–nickel single crystals. Ph.D. thesis, University of Minnesota, Minneapolis.

Dafermos, C., 1982. Global smooth solutions to the initial boundary value problem for the equations of one-dimensional nonlinear thermoviscoelasticity. SIAM Journal of Mathematical Analysis 13, 397–408.

Dafermos, C., Hsiao, L., 1982. Global smooth thermomechanical processes in one-dimensional nonlinear thermoviscoelasticity. Nonlinear Analysis T.M.A. 6, 435–454.

Ericksen, J., 1975. Equilibrium of bars. Journal of Elasticity 5, 191–202.

Făciu, C., 1996a. Initiation and growth of strain bands in rate-type viscoelastic materials. Part I. Discontinuous strain solutions. European Journal of Mechanics A/Solids 15 (6), 969–988.

Făciu, C., 1996b. Initiation and growth of strain bands in rate-type viscoelastic materials. Part II: The energetics of the banding mechanism. European Journal of Mechanics A 15 (6), 989–1011.

Făciu, C., 2001. On modelling phase propagation in SMAs by a Maxwellian thermo-viscoelastic approach. International Journal of Solids and Structures (in this volume).

Făciu, C., Suliciu, I., 1994. A Maxwellian model for pseudoelastic materials. Scripta Metallurgica 31, 1399–1404.

Fonseca, I., Brandon, D., Swart, P., 1994. Dynamics and oscillatory microstructure in a model of displacive phase transformations. In: Progress in Partial Differential Equations: The Metz Surveys 3, pp. 130–144.

Friesecke, G., McLeod, J., 1996. Dynamics as a mechanism preventing the formation of finer and finer microstructure. Archive for Rational Mechanics and Analysis 133, 199–247.

Friesecke, G., McLeod, J., 1997. Dynamic stability of non-minimizing phase mixtures. Proceedings of Royal Society of London A 453, 2427–2436.

James, R., 1980. The propagation of phase boundaries in elastic bars. Archive for Rational Mechanics and Analysis 73, 125–157.

James, R., 1992. Deformation of shape-memory materials. In: Liu, C., Kunsmann, H., Otsuka, K., Wuttig, M. (Eds.), Materials Research Society Symposium Proceedings, vol. 246, pp. 81–90.

Jiang, S., 1993. Global large solutions to initial boundary value problems in one-dimensional nonlinear thermoviscoelasticity. Quarterly Applied Mathematics 51, 731–744.

Kalies, W., 1994. Regularized models of phase transformation in one-dimensional nonlinear elasticity. Ph.D. thesis, Cornell University.

Krishnan, R., 1985. Stress induced martensitic transformations. Materials Science Forum 3, 387–398.

Krishnan, R., Brown, L., 1973. Pseudo-elasticity and the strain-memory effect in a Ag-45 at.pct. Cd alloy. Metallurgical Transactions 4, 423–429.

Leo, P., Shield, T., Bruno, O., 1993. Transient heat transfer effects on the pseudoelastic behavior of shape-memory wires. Acta Metallurgica et Materialia 41 (8), 2477–2485.

Li, D., Feng, Z., 1997. Dynamic properties of pseudoelastic shape memory alloys. SPIE 3041, 715–725.

Nakanishi, N., 1975. Lattice softening and the origin of SME. In: Perkins, J. (Ed.), Shape Memory Effects in Alloys. AIME, pp. 147–175.

Ngan, S.-C., Truskinovsky, L., 1999. Thermal trapping and kinetics of martensitic phase boundaries. Journal of the Mechanics and Physics of Solids 47, 141–172.

Pego, R., 1987. Phase transitions in one-dimensional nonlinear viscoelasticity: Admissibility and stability. Archive for Rational Mechanics and Analysis 97, 353–394.

Racke, R., Zheng, S., 1997. Global existence and asymptotic behavior in nonlinear thermoviscoelasticity. Journal of Differential Equations 134 (1), 46–67.

Shaw, J., 2000. Simulations of localized thermo-mechanical behavior in a NiTi shape memory alloy. International Journal of Plasticity 16, 541–562.

Shaw, J., Kyriakides, S., 1995. On the thermomechanical behavior of NiTi. Journal of the Mechanics and Physics of Solids 43, 1243–1281.

Shield, T.W., 1995. Orientation dependence of the pseudoelastic bahavior of single crystals of Cu–Al–Ni in tension. Journal of the Mechanics and Physics of Solids 43 (6), 869–895.

Swart, P., 1991. The dynamical creation of microstructure in material phase transitions. Ph.D. thesis, Cornell University.

Theil, F., 1998. Young-measure solutions for a viscoelastically damped wave equation with nonmonotone stress–strain relation. Archive for Rational Mechanics and Analysis 144, 47–78.

Truskinovsky, L., 1994. About the "normal growth" approximation in the dynamic theory of phase transitions. Continuum Mechanics and Thermodynamics 6, 185–208.

Vainchtein, A., Rosakis, P., 1999. Hysteresis and stick–slip motion of the interfaces in dynamic models of phase transitions. Journal of Nonlinear Science 9 (6), 697–719.